

# Spectral characterisation of offset pulse position modulation

ISSN 1751-8768


Received on 24th April 2014

Revised on 31st August 2014

Accepted on 2nd February 2015

doi: 10.1049/iet-opt.2014.0035

www.ietdl.org

Indrani Ray, Martin J. N. Sibley , Peter J. Mather

Department of Engineering and Technology, University of Huddersfield, UK, HD1 3DH

✉ E-mail: m.j.n.sibley@hud.ac.uk

**Abstract:** Offset pulse position modulation (PPM) has been shown to be more attractive for use in optical fibre channels than on–off keying, digital PPM and in some respects multiple PPM in some applications. However the spectral analysis of this coding scheme has not yet been addressed. In this study the authors present, for the first time, the spectral characteristics of an offset PPM sequence. The results show strong frequency components at the frame rate and, if return-to-zero pulses are used, the slot rate.

## 1 Introduction

Digital pulse position modulation (digital PPM) has been proposed as a way to trade the bandwidth available on the optical channel for an increase in signal to noise ratio [1]. Practical work has confirmed the theoretical predictions and measurements have shown that digital PPM gives an increase in receiver sensitivity of 4.5 dB when compared with on–off keying [2]. Unfortunately the benefits of digital PPM come at the expense of an increased line rate which can be prohibitively high. This led researchers to consider variations on digital PPM that offer the same sensitivity benefits but at a lower line rate.

Many different coding schemes have been proposed that offer a lower line rate. Shiu and Kahn [3] described differential PPM which suppresses the empty slots following the digital PPM pulse. A similar variant is digital pulse interval modulation (digital PIM) in which the empty slots preceding a pulse are suppressed. Both schemes offer a reduction in line rate but this comes at the expense of increased complexity as buffers are required at both the coder and the decoder. In the scheme known as dual header PIM (DH-PIM) a variable word length is used to reduce the line rate [4, 5]. Again, buffers are required in the coder and decoder.

Frame synchronisation is a problem with these modulation schemes as the frame length is variable. A modulation format that does not require buffers, and that has a spectral line at the frame rate, is the bandwidth-efficient code multiple PPM [6, 7]. In this modulation format, two or more pulses are used within a frame with the position of the pulses being governed by the original data. As will be seen later, this coding technique exhibits a spectral line at the frame repetition rate. A variation is shortened PPM [8, 9] in which the frame is divided up into  $(1 + 2^{M-1})$  slots where  $M$  is the number of data bits to be encoded. The first slot is reserved for the first data bit and the remaining slots are filled as per digital PPM. As shown by Cryan [9] the modulation scheme gives a spectral line at frame rate. Table 1 shows how three bits of data are coded by these modulation formats.

All of these schemes have their relative advantages and disadvantages and it was to counter the disadvantages that offset PPM was invented [10]. In offset PPM the most significant bit (MSB) is used to register the offset from a datum code, either 000 or 100 when coding three bits of data. The code alphabet is shown in Table 1. Ray *et al.* [11] have shown that offset PPM offers a 3.27 dB advantage over digital PPM and a lower bandwidth. It also gives better sensitivity than multiple PPM when the channel bandwidth is high. However, if the channel bandwidth is lower, the error rate increases because of inter-symbol interference (ISI)

and inter-frame interference (IFI). The effect of ISI and IFI can be reduced by using proper pulse shaping.

This paper presents the spectral analysis of offset PPM and a comparison between theoretical and numerical results is given. We will show that the spectrum contains discrete components at the slot repetition rate. Slot synchronisation has been taken into consideration for the first time as the offset PPM spectrum exhibits a discrete slot rate component. The effect of pulse shaping and modulation index on the spectrum is also presented. Frame synchronisation has also been considered for offset PPM as this coding scheme exhibits a strong frame rate component. The dependency of this frame component on the modulation index is examined. A comparison of the spectral characteristics of digital, multiple and shortened PPM is presented here. For ease of implementation an offset PPM coder has been designed. In this paper we have followed the approach introduced by Win [12].

## 2 Spectral characterisation

The spectral density function, or power spectrum, of a random sequence of signals is defined as the distribution of the average power with respect to frequency. Spectral analysis is important to the design of any system because it indicates one of the most important characteristics of a signal (i.e. bandwidth) and also the amount of total average power of that signal in any frequency band. The Fourier transform of the autocorrelation function of a signal gives the spectral density in the frequency domain.

An offset PPM sequence can be represented as

$$m(t) = \sum_{n=-\infty}^{\infty} a_n p(t - nT) \quad (1)$$

where  $\{a_n\}$  is the offset pulse sequence and  $p(t)$  is the pulse shape. To implement the probability distribution, 4-slot offset PPM was considered and 64 frames were taken randomly to form an offset data sequence. This data sequence was used to find out the probability distribution of zeros and ones using Matlab which is shown in Fig. 1.

The sequence can be made to have a zero mean,  $M(t)$ , as

$$M(t) = m(t) - \overline{m(t)} \quad (2)$$

**Table 1** Generation of different types of coding from equivalent 3 bits of data

OOK	Digital PPM	Differential PPM	Digital PIM	DH-PPM	Offset PPM	Shortened PPM	Multiple PPM
000	0000 0001	0000 0001	1	100	0000	0 0001	11000 (1,2)
001	0000 0010	0000 001	10	1000	0001	0 0010	10100 (1,3)
010	0000 0100	0000 01	100	1000 0	0010	0 0100	10010 (1,4)
011	0000 1000	0000 1	1000	1000 00	0100	0 1000	10001 (1,5)
100	0001 0000	0001	1 0000	1100 00	1000	1 0001	01100 (2,3)
101	0010 0000	001	10 0000	1100 0	1001	1 0010	01010 (2,4)
110	0100 0000	01	100 0000	1100	1010	1 0100	01001 (2,5)
111	1000 0000	1	1000 0000	110	1100	1 1000	00110 (3,4)

Here  $\overline{m(t)}$  is the mean of  $m(t)$  and is defined as

$$\overline{m(t)} \triangleq \mathbb{E}\{m(t)\} = \sum_{n=-\infty}^{\infty} \mathbb{E}\{a_n\} \mathbb{E}\{p(t-nT)\} \quad (3)$$

$\mathbb{E}\{\cdot\}$  represents the expected value. The autocorrelation function of the zero mean data sequence can be defined as (Appendix 1)

$$R_M(t; \tau) = \mathbb{E}\{M(t)M^*(t+\tau)\} \\ = \sum_{n=-\infty}^{\infty} \sum_{m=-\infty}^{\infty} \int_y \int_z K_a(n:m-n) \times P(y)P^*(z) \\ \times e^{-j2\pi y n T} e^{+j2\pi z m T} e^{+j2\pi(y-z)t} e^{-j2\pi z \tau} dy dz \quad (4)$$

where  $K_a(n:m-n) = \mathbb{E}\{a_n a_m^*\} - \mathbb{E}\{a_n\} \mathbb{E}\{a_m^*\}$ . Fig. 2 is the autocorrelation function of offset PPM data sequence.

In general the Power Spectral Density, PSD, of a digital pulse stream consists of both continuous and discrete components irrespective of the properties of the pulse stream  $a_n$ . Assume the pulse is a rectangular pulse of height  $A$ , pulse width  $t_p$  and offset PPM frame time  $T_f$ . According to Wiener–Khinchine theorem power spectral density is the Fourier transform of the autocorrelation function. The continuous spectrum (Appendix 2) of the offset PPM data sequence can be represented by using Wiener–Khinchine theorem [12] as

$$S_m^c(f) = \mathcal{F}\{\langle R_M(t;\tau) \rangle_\tau\} = S_a(f)S_p(f) \quad (5)$$

where  $\langle \cdot \rangle$  denotes time average for time duration  $t$ ,  $S_p(f)$  is the part of spectral component because of square pulse and  $S_a(f)$  is the part of spectral component because of data sequence  $a_n$ . Now, can be

calculated as follows

$$S_p(f) = \frac{1}{T} |P(f)|^2 = A t_p \text{sinc}\left(\frac{f t_p}{T_f}\right) \quad (6)$$

From (4)

$$S_a(f) = \sum_{l=-\infty}^{\infty} \left[ \frac{1}{N} \sum_{n=1}^N K_a(n:l) \right] e^{-j2\pi l T} \quad (7)$$

This term  $|P(f)|^2$ , in (6) represents the Fourier transform of the pulse shape  $p(t)$ . Combining (6) and (7) with (5), the final equation of the continuous spectrum can be written as

$$S_m^c(f) = A t_p \text{sinc}\left(\frac{f t_p}{T_f}\right) \sum_{l=-\infty}^{\infty} \left[ \frac{1}{N} \sum_{n=1}^N K_a(n:l) \right] e^{-j2\pi l T} \quad (8)$$

The discrete spectrum (Appendix 3) can be represented as

$$S_m^d(f) = \mathcal{F}\{\langle R_M(t;\tau) \rangle_\tau\} \\ = \frac{A}{T_f^2} \sum_{l=-\infty}^{\infty} \left| P\left(\frac{l}{T_f}\right) \right|^2 \times \left| \sum_{n=1}^N \mathbb{E}\{a_n\} e^{+j(2\pi/N)ln} \right|^2 \delta\left(f - \frac{l}{T_f}\right) \quad (9)$$

The term  $\sum_{n=1}^N \mathbb{E}\{a_n\} e^{+j(2\pi/N)ln}$  represents the characteristic function of the data distribution of the offset PPM sequence and  $T_f = (NT)$  is the total frame time.

### 3 Offset PPM coder design

The offset PPM coding scheme has been described in [10, 11] and illustrated in Table 1. To determine the spectral characteristic of

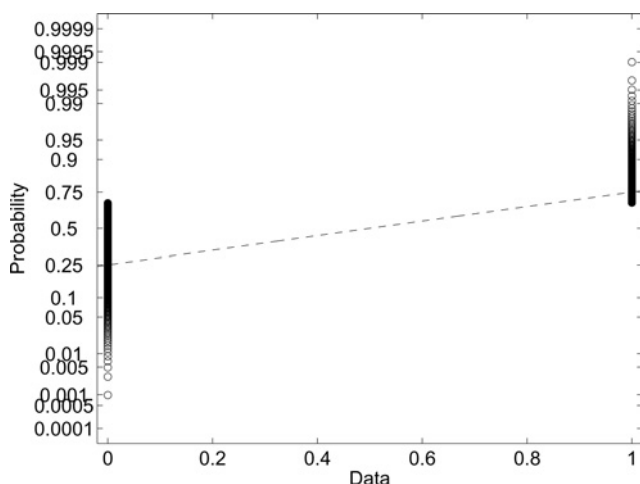


**Fig. 1** Probability distribution for 4-slot offset PPM

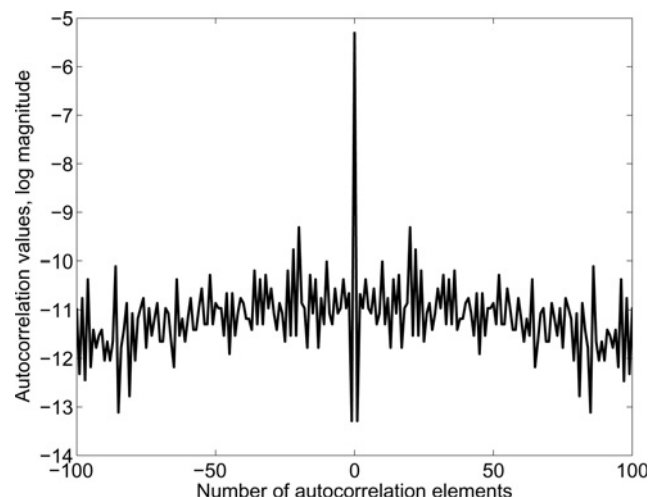


**Fig. 2** Autocorrelation for 4-slot offset PPM

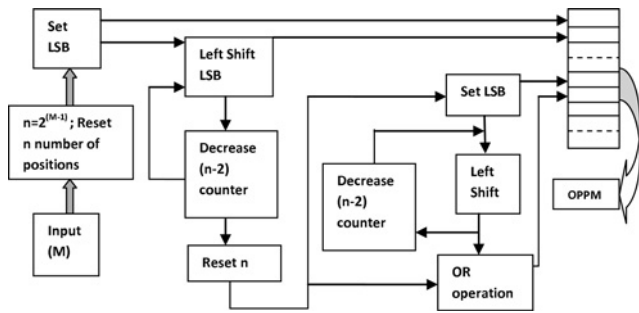


Fig. 3 Schematic diagram of the offset PPM coder

offset PPM, an offset PPM coder was designed using Matlab toolbox. For  $M$  number of pulses to be coded, the length of a codeword is  $n = 2^{M-1}$  where  $N = 2^M$  is the number of possible codewords in an offset PPM sequence. Table 1 shows how the codewords are generated in an offset PPM sequence. In offset PPM, all  $n$  positions of a codeword are initially reset to zero corresponding to the first codeword in the sequence. The second codeword in the sequence is obtained by setting the least significant bit (LSB) to one. Subsequent codewords in the sequence are produced by shifting the LSB to left until the MSB is reached. With reference to Fig. 3, the MSB is kept at one and the next codeword in the sequence is formed by setting the LSB to one. This is done by using the OR operation between the generated sequence and the output of the first loop to keep the MSB set. Subsequent codewords are formed by left shifting the LSB up to  $(n - 1)$  positions. A buffer is used to store all the codewords produced sequentially in each step. The output gives all the possible offset PPM codewords.

#### 4 Result and discussion

The PSD of offset PPM was evaluated both theoretically, using the results of Section 2, and numerically using the coder schematic and the fast Fourier transform. Eight samples per offset PPM slot were considered, 1024 frames were taken randomly and 50 FFT's were averaged to decrease the noise because of randomness of the data sequence and because of averaging, the variance was reduced from 0.1457 to 0.1154. X-axis has been normalised to frame rate by dividing the total number of slots and no data windowing was considered.

Fig. 4 shows the theoretical and numerically obtained PSD of offset PPM coding 4 bits of data (eight offset PPM data slots)

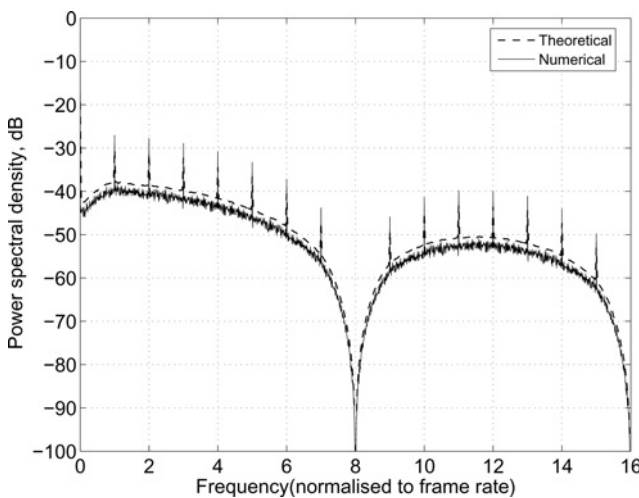


Fig. 4 Comparison of theoretical and numerically obtained power spectral density for offset PPM coding 4 bits of data using NRZ data

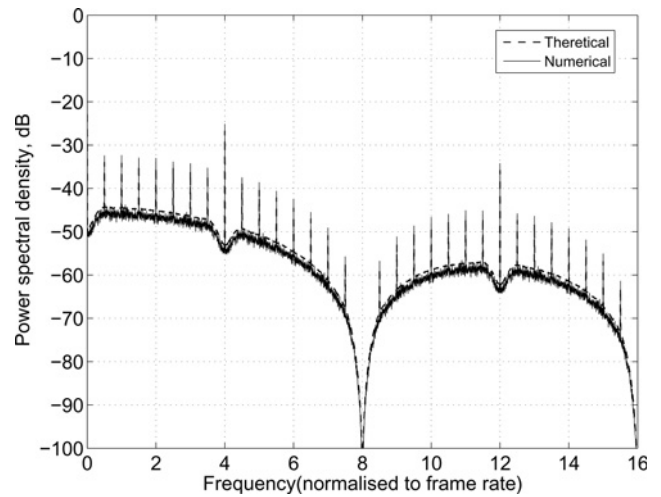


Fig. 5 Comparison of theoretical and numerically obtained power spectral density for offset PPM coding 4 bits of coding level using 50% duty cycle RZ data

using non-return-to-zero, NRZ, pulses. As can be seen, there is excellent agreement between theoretical and numerical results. There are seven distinct spectral components corresponding to the frame rate and its associated harmonics. There should be an eighth spectral line but, as is normal with NRZ signalling, there is a null in the spectrum corresponding to the frequency equal to the inverse of the pulse width and this coincides with the frequency of the missing line. To confirm this, Fig. 5 shows the spectrum obtained using 50% return-to-zero (RZ) pulses. As can be seen, the bandwidth is effectively doubled but there is a line at the slot frequency.

Figs. 6–8 show the numerically predicted PSD for digital, multiple and shortened PPM when coding 4 bits of data. As can be seen from Fig. 6 for digital PPM, there is no line at the frame rate (because of even distribution of the bits in the codewords) and no line at the slot frequency, as expected. A frequency component at the frame frequency can be generated if the digital PPM contains unmodulated guard slots at the end of the frame (see Section 4.2 later). Both multiple and shortened PPM (Figs. 7 and 8) show discrete lines at the frame frequency but no lines at the slot frequency because of the use of NRZ pulses. As all the results are represented for 4 bits of coding so, these figures can easily be compared in terms of line rate and bandwidth. Digital PPM gives maximum line rate among these four coding theory as it uses 16 slots to transfer 4 bits of data and as a result it uses maximum

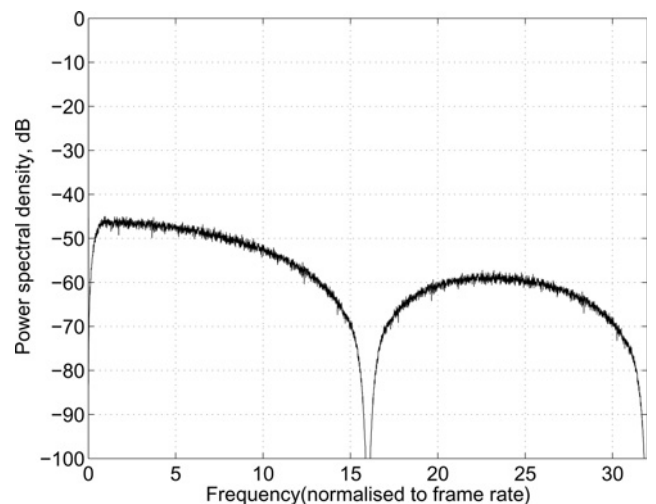


Fig. 6 Numerical PSD of digital PPM for coding 4 bits of data

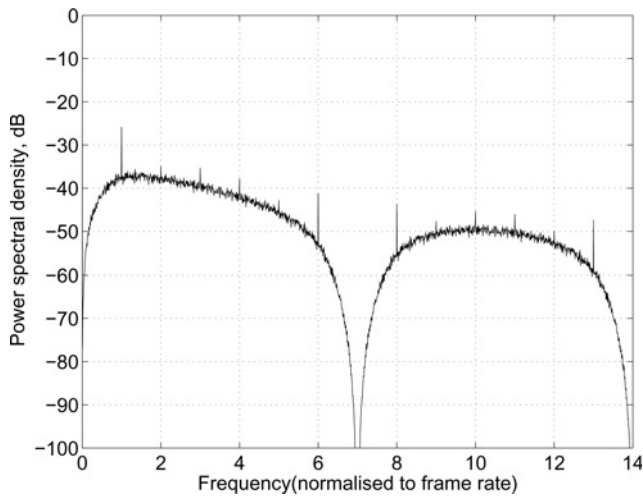


Fig. 7 Numerical PSD of multiple PPM for coding 4 bits of data

Table 2 Comparison of offset PPM, digital PPM and multiple PPM

Coding	Number of bits coded-coding level	DC value	Slot rate power	Frame rate power
offset	3	-10.1 dB	-19.16 dB	-24.12 dB
PPM	4	-15.23 dB	-25.16 dB	-26.82 dB
digital	3	-18.1 dB	-27.95 dB	-32.45 dB
PPM	4	-24.08 dB	-33.97 dB	-38.04 dB
multiple	3	-7.96 dB	-17.85 dB	-25.82 dB
PPM	4	-10.88 dB	-20.77 dB	-25.91 dB
shortened	3	-10.48 dB	-21.37 dB	-26.25 dB
PPM	4	-15.51 dB	-25.41 dB	-27.88 dB

bandwidth. Multiple PPM is the most bandwidth efficient code and it uses seven slots to transfer 4 bits of data and likewise shortened PPM uses nine slots and offset PPM uses eight slots.

## 5 Frame synchronisation

Frame components are mostly affected by data distribution on a frame and Table 2 compares the amplitude of the frame

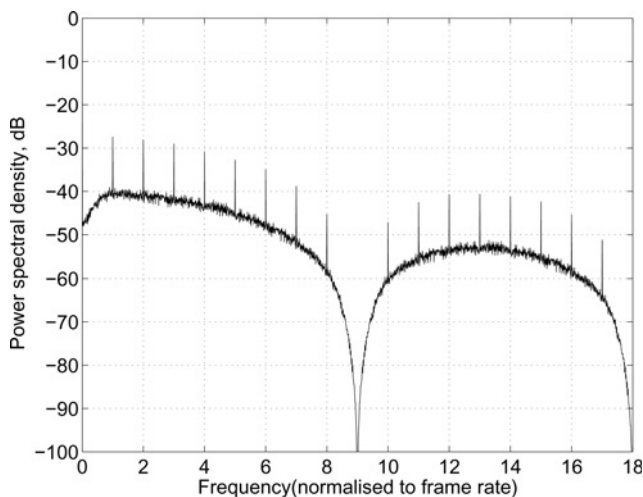


Fig. 8 Numerical PSD of shortened PPM for coding 4 bits of data

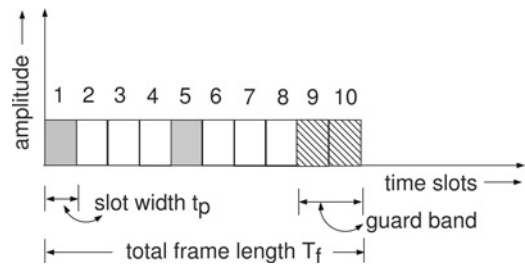


Fig. 9 Consideration of frames for modulation index 0.8

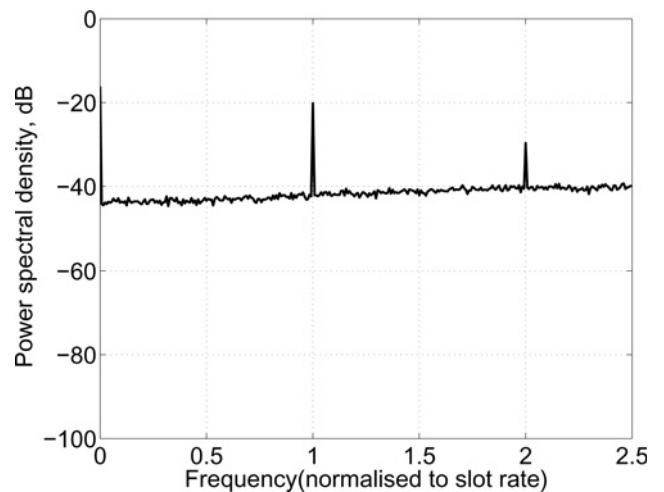


Fig. 10 PSD of offset PPM for frame synchronisation at modulating index = 0.5 and  $n = 4$

components for digital, multiple, shortened and offset PPM using NRZ pulses. Frame rate component is measured by the power at the first spike using non-return to zero pulse and the DC value is measured as the power at zero frequency. As previously discussed, the frame component in digital PPM is not present unless an empty guard interval is used. To obtain the frame component, a modulation index of 0.8 was used. The modulation index (Fig. 9) is defined by the ratio of the effective band to the total frame

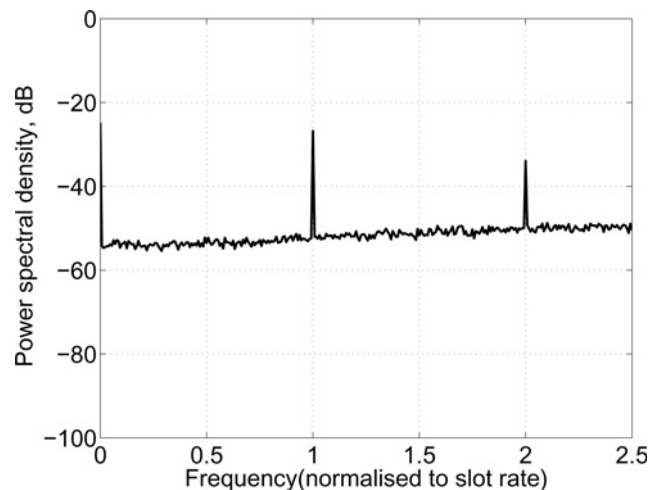
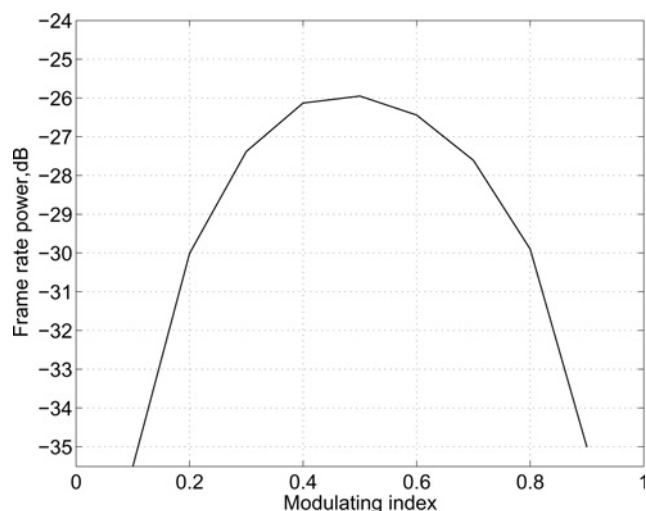


Fig. 11 PSD of offset PPM for frame synchronisation at modulating index = 0.5 and  $n = 8$



**Fig. 12** Offset PPM frame rate power with respect to modulating index when  $n = 8$

length and is given by

$$m = (nt_p)/T_f \quad (10)$$

As can be seen from Table 2, offset PPM has the frame component with the highest amplitude. It is also worth noting that offset PPM has the lowest bandwidth expansion and this eases implementation.

Figs. 10 and 11 show the change in frame rate power with a change in the modulating index;  $m = 0.5$  when  $n = 4$  for Fig. 10 and  $m = 0.5$  when  $n = 8$  for Fig. 11. In Fig. 12 is shown how frame rate power changes with variations in the modulating index. From this figure we can say that the frame rate power is a maximum at a modulating index of  $m = 0.5$ . Here x-axis has been normalised to slot rate by dividing the total length of signal to the number of slot.

## 6 Slot synchronisation

The strength of the slot clock is highly affected by the pulse shape (as already seen) and the modulation index. There are two ways to extract a slot clock from a PPM data stream: direct extraction of the slot clock; generation of the slot clock using a phase-lock-loop locked to the frame frequency. As discussed previously, the spectra of the PPM systems show a null at the slot frequency because of NRZ pulses being used. To extract the slot clock, the pulse width must be reduced to move this null to a higher frequency so that the slot clock can be extracted. Table 2 shows the amplitude of the slot component for all four codes using RZ pulses. In this case the slot clock would have to be produced and phase locked to the frame component. This area of work is subject to another investigation and will be reported on later.

**Table 3** DC value, slot rate power and frame rate power change with respect to coding level for offset PPM

Coding level of Offset PPM	DC value (dB) NRZ pulse	Slot rate power (dB) RZ pulse	Frame rate power (dB) NRZ pulse
3	-10.1	-19.16	-24.12
4	-15.23	-25.16	-26.82
5	-20.97	-30.76	-31.43
6	-26.75	-36.7	-36.69
7	-32.7	-42.62	-42.57
8	-38.7	-48.55	-48.18
9	-44.7	-54.57	-53.13
10	-50.72	-60.76	-60.09

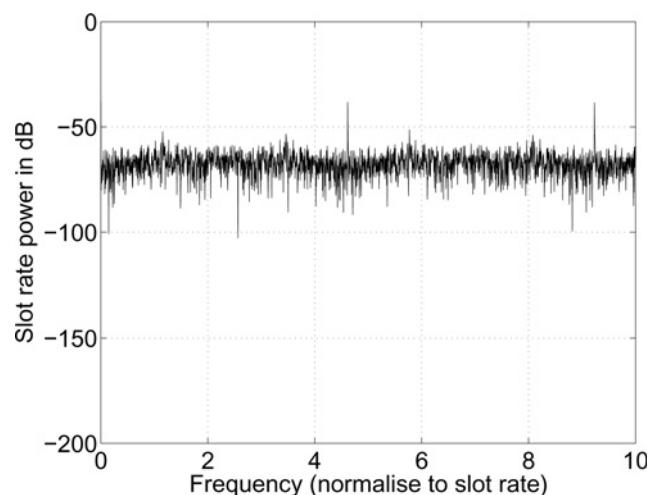


**Fig. 13** Slot rate component when  $n = 4$ ,  $m = 0.3$

Table 3 shows how the DC, slot component and frame component strengths vary with coding level (number of bits coded) for offset PPM. As can be seen, the power in all components reduces as more bits of data are encoded. This is to be expected as the interval between pulses increases.

If the length of the guard interval is increased, while keeping the total frame length fixed, the modulation index will reduce and the pulse width will be reduced. This will affect the spectrum. A practical four slot offset PPM was evaluated considering 50% duration of the pulse and modulating index  $m = 0.3$ . The numerically predicted result is shown in Fig. 13. The spectrum shows the presence of discrete slot rate components. The pulse shaping effect and the continuum because of the data randomness are also clear.

## 7 Conclusions

This paper has examined and compared the spectral characteristics of offset, digital, multiple and shortened PPM. Theoretical predictions of the power spectral density of offset PPM have shown excellent agreement with simulation results.

Examination of the PSD has shown that digital PPM does not give a discrete line at the frame repetition frequency, whereas offset, multiple and shortened PPM do. This component can be extracted to obtain the slot clock needed to regenerate the signal. It has been shown that offset PPM has the strongest frame component.

## 8 Acknowledgment

The authors would like to thank Professor Bob Cryan of the University of Huddersfield for some useful discussion and comments.

## 9 References

- Garrett, I.: 'Pulse-position modulation for transmission over optical fibres with direct or heterodyne detection', *IEEE Trans.*, 1983, **COM-31**, pp. 518–527
- Calvert, N.M., Sibley, M.J.N., Unwin, R.T.: 'Experimental optical fibre digital pulse-position modulation system', *Electron. Lett.*, 1988, **24**, (2), pp. 129–131
- Shiu, D.S., Kahn, J.M.: 'Differential pulse-position modulation for power-efficient optical communication', *IEEE Trans. Commun.*, 1999, **47**, (8), pp. 1201–1210
- Aldibbiat, N.M., Ghassemlooy, Z., McLaughlin, R.: 'Error performance of dual header pulse interval modulation (DH-PIM) in optical wireless communications', *IEE Proc. Optoelectron.*, 2001, **16**, (2), pp. 91–96
- Aldibbiat, N.M., Ghassemlooy, Z., McLaughlin, R.: 'Dual header pulse interval modulation for dispersive indoor optical wireless communication systems', *IEE Proc. Circuits Devices Syst.*, 2002, **146**, (3), pp. 187–192
- Sugiyama, H., Nosu, K.: 'MPPM: a method for improving the band-utilization efficiency in optical PPM', *J. Lightw. Technol.*, 1989, **7**, (3), pp. 465–472

- 7 Nikolaidis, K., Sibley, M.J.N.: 'Investigation of an optical multiple PPM link over a highly dispersive optical channel', *IET Optoelectron.*, 2007, **1**, (3), pp. 113–119.
- 8 Sui, M., Yu, X., Zhang, F.: 'The modified PPM modulation for underwater wireless optical communication'. *IEEE Int. Conf. on Communication Software and Networks*, 2009, pp. 173–177
- 9 Cryan, R.A.: 'Spectral characterization of shortened PPM format', *Electron. Lett.*, 2010, **46**, (5), pp. 355–356
- 10 Sibley, M.: 'Analysis of offset pulse position modulation- a novel reduced bandwidth coding scheme', *IEE Proc. Optoelectron.*, 2011, **5**, (4), pp. 144–150
- 11 Ray, I., Sibley, M.J.N., Mather, P.J.: 'Performance analysis of offset pulse position modulation over optical channel', *IEEE J. Lightw. Technol.*, 2012, **30**, (3), pp. 144–150
- 12 Win, M.Z.: 'On the power spectral density of digital pulse streams generated by M-ary Cyclostationary sequences in the presence of stationary timing jitter', *IEEE Trans. Commun.*, 1998, **46**, (9), pp. 1135–1145

## 10 Appendix

### 10.1 Appendix 1

The correlation function [12] of the zero mean process  $M(t)$  is given by

$$R_M(t; \tau) = \mathbb{E}\{M(t)M^*(t + \tau)\}$$

$$= \mathbb{E}\left\{\sum_{n=-\infty}^{\infty} [a_n p(t - nT) - \mathbb{E}\{a_n\}\mathbb{E}\{p(t - nT)\}] \times \sum_{m=-\infty}^{\infty} [a_m p(t + \tau - mT) - \mathbb{E}\{a_m\}\mathbb{E}\{p(t + \tau - mT)\}]^*\right\} \quad (11)$$

This can be rewritten as

$$R_M(t; \tau) = \sum_{n=-\infty}^{\infty} \sum_{m=-\infty}^{\infty} \mathbb{E}\{a_n a_m^* p(t - nT) p^*(t + \tau - mT)\} - \mathbb{E}\{a_n\}\mathbb{E}\{a_m^*\} \times \mathbb{E}\{p(t - nT)\}\mathbb{E}\{p^*(t + \tau - mT)\} \quad (12)$$

Since

$$p(t) = \int_{-\infty}^{\infty} P(f) e^{+j2\pi ft} df \quad (13)$$

where  $P(f)$  is the Fourier transform of  $p(t)$ . Substituting (13) into (12) gives

$$R_M(t; \tau) = \sum_{n=-\infty}^{\infty} \sum_{m=-\infty}^{\infty} \int_y \int_z [\mathbb{E}\{a_n a_m^*\} - \mathbb{E}\{a_n\}\mathbb{E}\{a_m^*\}] \times P(y)P^*(z) e^{-j2\pi y n T} e^{+j2\pi z m T} e^{+j2\pi(y-z)t} e^{-j2\pi z \tau} dy dz \quad (14)$$

Now the Kernel is defined as

$$K_a(n; m - n, -y, -z) \triangleq \mathbb{E}\{a_n a_m^*\} - \mathbb{E}\{a_n\}\mathbb{E}\{a_m^*\} \quad (15)$$

Using the definition of Kernel, the autocorrelation function becomes

$$R_M(t; \tau) = \sum_{n=-\infty}^{\infty} \sum_{m=-\infty}^{\infty} \int_y \int_z K_a(n; m - n, -y, -z) \times P(y)P^*(z) e^{-j2\pi y n T} e^{+j2\pi z m T} e^{+j2\pi(y-z)t} e^{-j2\pi z \tau} dy dz \quad (16)$$

### 10.2 Appendix 2

The continuous PSD [12] of  $m(t)$  is given by

$$S_m^c(f) = \mathcal{F}_{\mathcal{T}}\{\langle R_M(t; \tau) \rangle_{\tau}\}$$

$$= \sum_{n=-\infty}^{\infty} \sum_{m=-\infty}^{\infty} \int_y \int_z K_a(n; m - n, -y, -z) P(y)P^*(z) \times e^{-j2\pi y n T} e^{+j2\pi z m T} \underbrace{\langle e^{+j2\pi(y-z)t} \rangle_{\mathcal{T}}}_{\delta(f+z)} dy dz$$

$$= \int_y \sum_{n=-\infty}^{\infty} \sum_{m=-\infty}^{\infty} K_a(n; m - n, -y, f) P(y)P^*(-f) \times e^{-j2\pi y n T} e^{-j2\pi f m T} \langle e^{+j2\pi(y+f)t} \rangle dy \quad (17)$$

$$= \int_y \sum_{n=-\infty}^{\infty} \sum_{m=-\infty}^{\infty} K_a(n; m - n, -y, f) P(y)P^*(-f) \times e^{-j2\pi f(m-n)T} e^{-j2\pi(y+f)nT} \langle e^{+j2\pi(y+f)t} \rangle dy$$

Letting  $l = (m - n)$ ,  $K_a(n; l, -y, f)$  is periodic in  $n$  with period  $N$  for a WSCS sequence, it can be easily shown that

$$\sum_{n=-\infty}^{\infty} K_a(n; l, -y, f) e^{-j2\pi(y+f)nT}$$

$$= \sum_{n=1}^N K_a(n; l, -y, f) e^{-j2\pi(y+f)nT} \sum_{i=-\infty}^{\infty} e^{-j2\pi(y+f)iNT} \quad (18)$$

Using Poisson sum formula

$$\sum_{n=-\infty}^{\infty} e^{-j2\pi x n T} = \frac{1}{T} \sum_{k=-\infty}^{\infty} \delta\left(x - \frac{k}{T}\right) \quad (19)$$

and integrating over  $y$ , (17) becomes

$$S_m^c(f) = \sum_{k=-\infty}^{\infty} \sum_{l=-\infty}^{\infty} \frac{1}{NT} \sum_{n=1}^N K_a\left(n; l, f - \frac{k}{NT}, f\right) \times P\left(-f + \frac{k}{NT}\right) P^*(-f) e^{-j2\pi m(k/N)} e^{-j2\pi f l T} \langle e^{j2\pi(k/NT)t} \rangle \quad (20)$$

For a real pulse shape  $p(t)$ ,  $|P(f)| = |P(-f)|$  and also

$$\langle e^{j2\pi(k/NT)t} \rangle = \frac{1}{NT} \int_{-(NT/2)}^{(NT/2)} e^{j2\pi(k/NT)t} dt = \begin{cases} 1, & k = 0 \\ 0, & k \neq 0 \end{cases} \quad (21)$$

Therefore equations for continuous spectrum becomes

$$S_m^c(f) = \frac{1}{T} |P(f)|^2 \sum_{l=-\infty}^{\infty} \left[ \frac{1}{N} \sum_{n=1}^N K_a(n; l) \right] e^{-j2\pi f l T} \quad (22)$$

### 10.3 Appendix 3

The discrete PSD [12] of  $m(t)$  is given by

$$\begin{aligned}
 S_m^d(f) &= \mathcal{F}_T \left\{ \left\langle \sum_{n=-\infty}^{\infty} \sum_{m=-\infty}^{\infty} \mathbb{E}\{a_n\} \mathbb{E}\{p(t-nT)\} \right. \right. \\
 &\quad \left. \left. \times \mathbb{E}\{a_m^*\} \mathbb{E}\{p^*(t+\tau-mT)\} \right\rangle \right\} \\
 &= \mathcal{F}_T \left\{ \sum_{n=-\infty}^{\infty} \sum_{m=-\infty}^{\infty} \mathbb{E}\{a_n\} \mathbb{E}\{a_m^*\} \right. \\
 &\quad \times \left\langle \mathbb{E} \left\{ \int_y P(y) e^{-j2\pi y n T} e^{+j2\pi y t} dy \right\} \right. \\
 &\quad \left. \times \mathbb{E} \left\{ \int_z P^*(z) e^{-j2\pi z \tau} e^{+j2\pi z m T} e^{-j2\pi z t} dz \right\} \right\rangle \left. \right\} \\
 &= \int_y \int_z \sum_{n=-\infty}^{\infty} \sum_{m=-\infty}^{\infty} \mathbb{E}\{a_n\} \mathbb{E}\{a_m^*\} \\
 &\quad \times P(y) P^*(z) \times e^{-j2\pi y n T} e^{+j2\pi z m T} \\
 &\quad \times \underbrace{\langle e^{+j2\pi(y-z)t} \rangle}_{\delta(f+z)} \mathcal{F}_T \{ e^{-j2\pi z \tau} \} dy dz \quad (23)
 \end{aligned}$$

Integrating over  $z$  and rearranging terms gives

$$\begin{aligned}
 S_m^d(f) &= \int_y \sum_{n=-\infty}^{\infty} \mathbb{E}\{a_n\} e^{-j2\pi y n T} \sum_{m=-\infty}^{\infty} \mathbb{E}\{a_m^*\} e^{-j2\pi f m T} \\
 &\quad \times P(y) P^*(-f) \langle e^{+j2\pi(y+f)t} \rangle dy \quad (24)
 \end{aligned}$$

$\mathbb{E}\{a_n\}$  is periodic in  $n$  with period  $N$ , hence

$$\sum_{n=-\infty}^{\infty} \mathbb{E}\{a_n\} e^{-j2\pi y n T} = \sum_{n=1}^N \mathbb{E}\{a_n\} e^{-j2\pi y n T} \times \sum_{i=-\infty}^{\infty} e^{-j2\pi y i N T} \quad (25)$$

Using this together with the Poisson sum formula given in (19) and integrating over  $y$  the above expression becomes

$$\begin{aligned}
 S_m^d(f) &= \frac{1}{NT} \sum_{k=-\infty}^{\infty} \sum_{n=1}^N \mathbb{E}\{a_n\} e^{-j2\pi(kn/N)} \\
 &\quad \times \frac{1}{NT} \sum_{l=-\infty}^{\infty} \sum_{m=1}^N \mathbb{E}\{a_m^*\} e^{-j2\pi(lm/N)} \delta\left(f - \frac{l}{NT}\right) \\
 &\quad \times P\left(\frac{k}{NT}\right) \times P^*\left(-\frac{l}{NT}\right) \langle e^{+j2\pi(k+l/NT)t} \rangle \quad (26)
 \end{aligned}$$

Using (21) the above expression reduces to

$$\begin{aligned}
 S_m^d(f) &= \frac{1}{(NT)^2} \sum_{l=-\infty}^{\infty} \left| P\left(\frac{l}{NT}\right) \right|^2 \\
 &\quad \times \left| \sum_{n=1}^N \mathbb{E}\{a_n\} e^{+j2\pi(nl/N)} \right|^2 \delta\left(f - \frac{l}{NT}\right) \quad (27)
 \end{aligned}$$

Copyright of IET Optoelectronics is the property of Institution of Engineering & Technology and its content may not be copied or emailed to multiple sites or posted to a listserv without the copyright holder's express written permission. However, users may print, download, or email articles for individual use.